Dear Associate Editor and reviewers:

Thanks again for all comments and suggestions to the paper. Please see my detailed response bellow.

Yaxun Tang

Associate Editor

1. Some equations have been changed (including summations over $\mathbf{p}_r$ and $\mathbf{p}_s$) to make the theory more consistent. Please see the revised manuscript.

2. More figures have been included to show the improvement in resolution. Probably the claims of much better resolution is too strong, but I think the inverted result does show some improvement in both resolution and amplitudes. I replaced the corresponding statement with "slightly improved resolution".

3. The comments indicated by Associate Editor in the annotated manuscript were also taken into consideration and included in the revised version.

Reviewer 1

1. I appreciate the suggestions that reviewer 1 made on the equations. However, the equation that he proposed is not what I am exactly doing, although it is pretty close. Let us only consider encoding receiver-side Green's functions, a similar discussion for the simultaneous encoding easily follows. My method only introduces crosstalk when $\mathbf{x}_r \neq \mathbf{x}'_r$ and I show that by stacking over $\mathbf{p}_r$, these crosstalk terms can be (approximately) canceled out. However, the equation reviewer 1 suggested introduces crosstalk when either $\mathbf{x}_r \neq \mathbf{x}'_r$, or $\mathbf{p}_r \neq \mathbf{p}'_r$, so basically his equation contains much more cross terms than mine, and it is not what I am exactly doing in this paper. But I agree that including the summation over $\mathbf{p}_r$ may make the story more consistent, and I have made corresponding changes in the revised manuscript. One thing I think I have to emphasize is that the plane-wave encoding function $\sum_{\mathbf{p}_r} a(\mathbf{x}_r, \mathbf{p}_r, \omega) a^*(\mathbf{x}'_r, \mathbf{p}_r, \omega) = \sum_{\mathbf{p}_r} A_r^2(\omega) e^{-i\omega \mathbf{p}_r (\mathbf{x}'_r - \mathbf{x}_r)}$ converges to a delta function $\delta(\mathbf{x}'_r - \mathbf{x}_r)$ asymptotically, and hence it satisfies the condition $\sum_{\mathbf{p}_r} |a(\mathbf{x}_r, \mathbf{p}_r, \omega)|^2 = 1$ asymptotically, this has also been elaborated in the revised manuscript.

2. I have added a sentence to explain $\mathbf{H}^{-1}$ cannot be obtained exactly and changed the notation for adjoint to *.

3. I have included a square for the L2 norm.

Reviewer 2

1. I really wish I could show some 3-D examples in this paper. However, the computer resources are limited in universities and moving towards 3-D is still a gradual and on-going process. Since 3-D field examples are required for students at Stanford Exploration Project to graduate, I also wish I could have the examples as soon as possible so that I can graduate faster :-). I think 3-D examples would be included in a separate paper. For the cost comparison, I think even the examples are in 2-D, the cost estimate in 3-D is of interest and can be easily predicted. Demonstrating the savings in 3-D would further motivate the application of this method to 3-D cases.

2. The normalized migration (Figure 11 or Figure 12) does not help to improve the resolution of the image because the diagonal of the Hessian only serves as a scaling factor, it has little deconvolution effects. Of course, one can use AGC to boost up the amplitude, but there is little physics in doing so for depth migrated images. Normalizing with the Hessian, on the other hand, has clear physical meaning and the amplitude is more reliable. The resolution can be improved by using the off-diagonal elements of the Hessian matrix. I have elaborated this in the revised manuscript.

3. My criteria for judging resolution is by looking at its spectrum: if the resolution improves, the image should have a broader range of frequency spectrum, or equivalently, the spatial domain representation should be crisper and sharper (or weaker sidelobes, if you want). I think the inverted image is sharper and crisper than the migrated image, thus I think the resolution is improved. I have to admit that the improvement is not very significant as complained by reviewer 2 (I have made corresponding changes in the revised manuscript), but considering the difficulty in subsalt areas and especially this particular model (extremely poor illumination in some subsalt area due to the rugosity of the top salt), a little improvement is always important and beneficial. Besides, I think the inverted image shows clearer sediment and fault truncations against the salt (indicated by circles and arrows in the revised manuscript). These truncations are important for locating subsalt structural traps, which are crucial for successful subsalt explorations. I show more figures as follows to better compare the migrated image and the inverted image. Figure 1 compares the vertical trace at horizontal distance 9.1135 km (slicing through one of the point diffractors) extracted from the images shown in Figure 14 in the revised manuscript. The inverted result (red dashed line) shows slightly weaker sidelobes than the migrated result (blue solid line). Figure 2 shows a closeup look around the point diffractors. Figure 3 compares the frequency spectrum of the migrated image and the inverted image from Figure 2. We can see that the inverted image has a broader range of the spatial frequencies, suggesting slightly improved spatial resolution. Figure 4 compares the horizontal trace at depth 5.1892 (slicing through the diffractors) extracted from Figure 2. It is quite clear that the inverted result better predicts the true reflectivity.

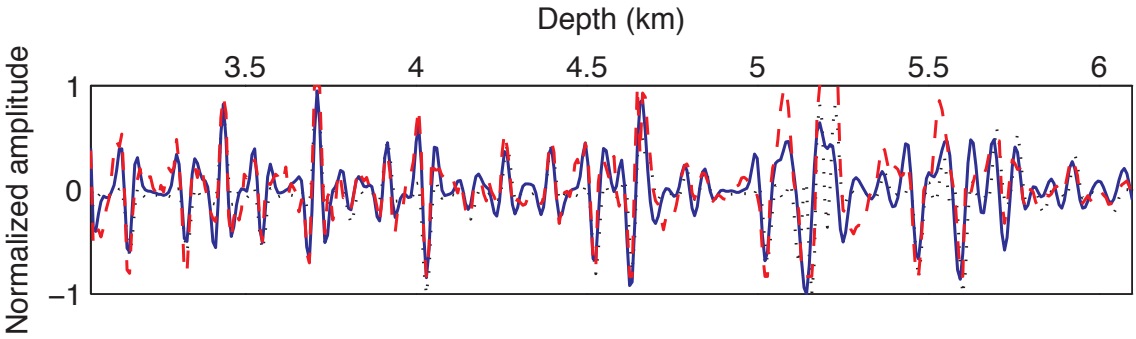

Figure 1: A vertical trace located at horizontal distance 9.1135 km extracted from images shown in Figure 14. Black dotted line, blue solid line and red dashed line represent traces extracted from the true reflectivity model, the migrated image and the inverted image, respectively.

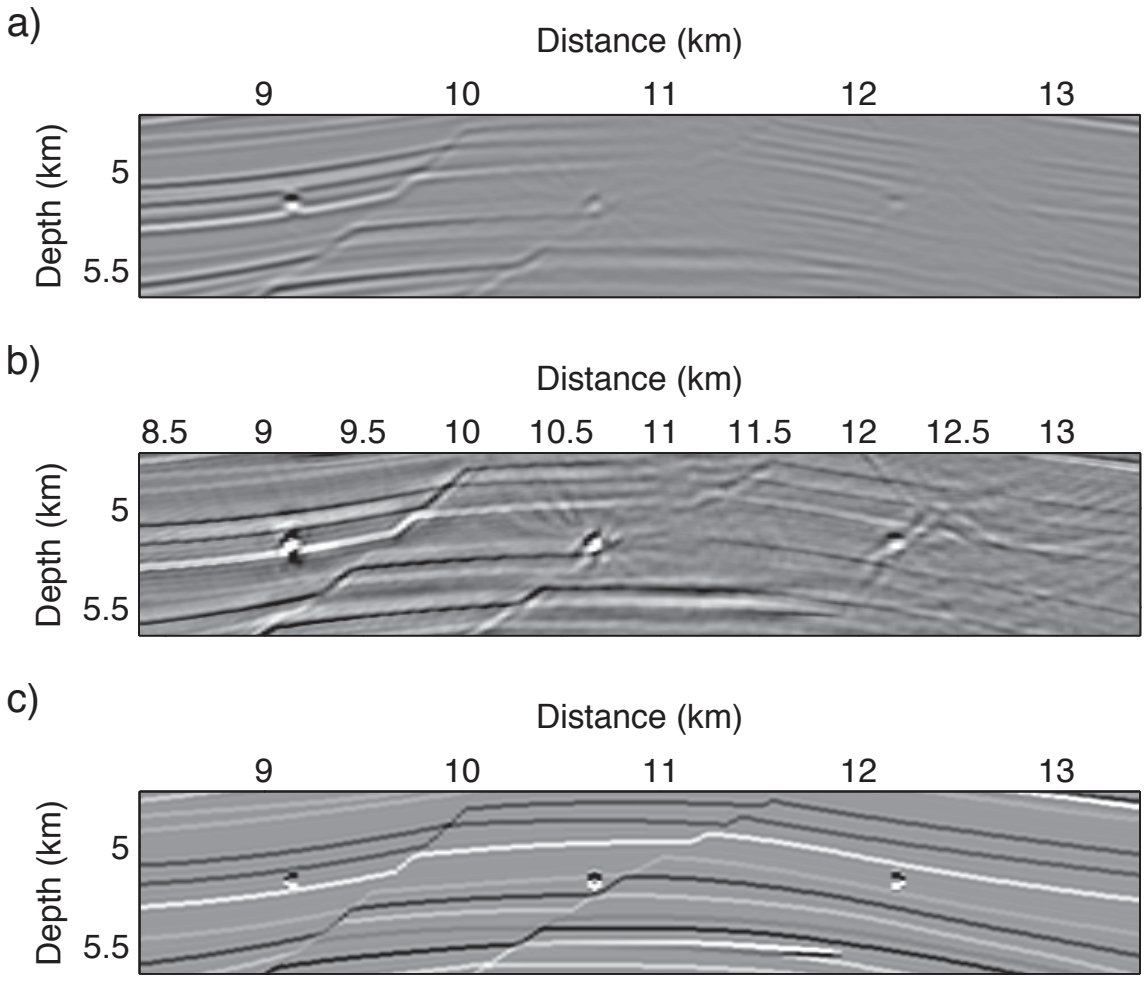

Figure 2: A closeup view of (a) the migrated image, (b) the inverted image and (c) the filtered true reflectivity model.

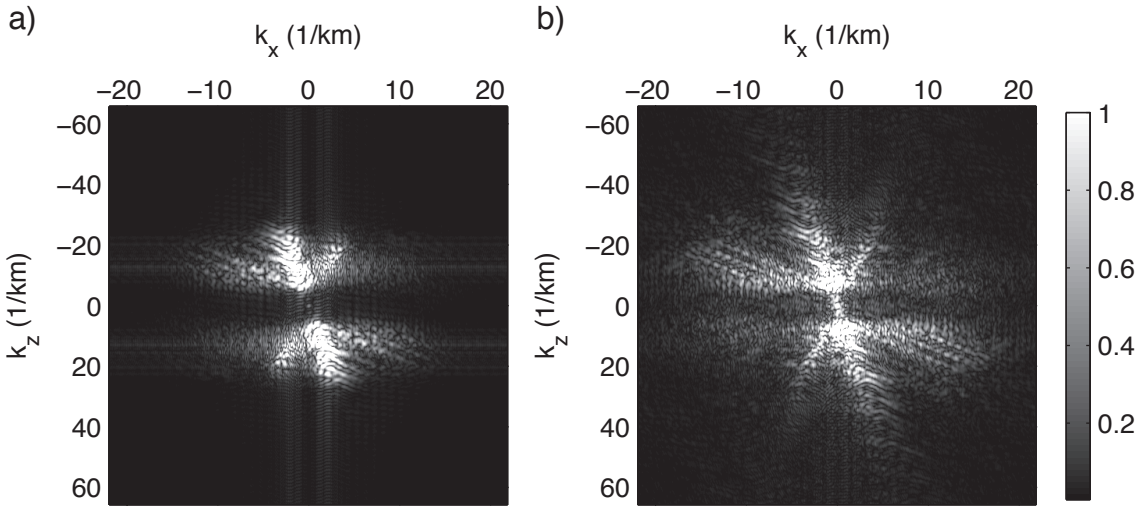

Figure 3: The amplitude spectrum of (a) the migrated image (Figure 2(a)) and (b) the inverted image (Figure 2(b)). Note the inverted image contains a broader range of spatial frequencies.

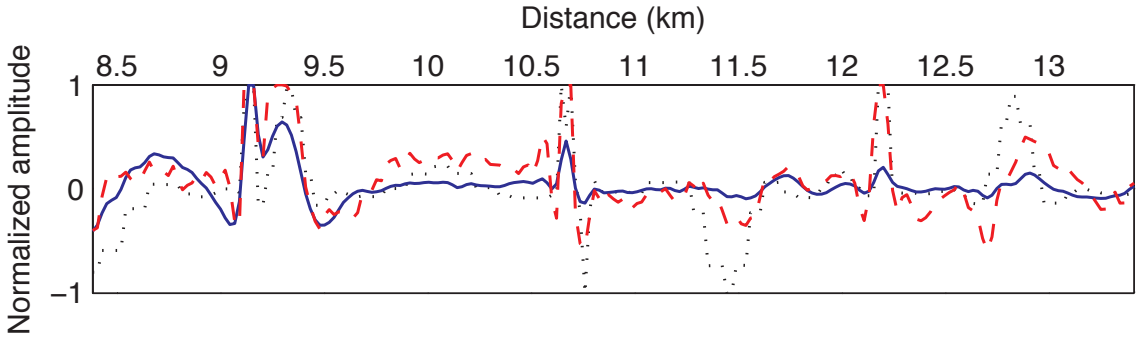

Figure 4: A horizontal trace located at depth 5.1892 km extracted from images shown in Figure 2. Black dotted line, blue solid line and red dashed line represent traces extracted from the true reflectivity model, the migrated image and the inverted image, respectively.